ORIGINAL ARTICLE

Investigation of high speed cutting performance and phase transformation behavior of NiTi shape memory alloys

Eren Kaya[1] · İrfan Kaya[1]

Abstract

This paper aims to investigate the high-speed machinability and phase transformation behavior of nickel-titanium shape memory alloys considering the process and post-process perspective. The tool wear results showed that PCD tool has great potential over carbide considering the limitation of quick tool wear in the high cutting speed range. Maximum tool life was achieved at the cutting speed of 130 m/min. The results obtained from differential scanning calorimetry indicated that the latent heats and transformation temperatures of nickel-titanium shape memory alloy are highly cutting speed dependent. Decrease of the cutting speed resulted in increased impair on these properties. It was found that the decrease of the cutting speed causes a decrease in the transformation enthalpy. The results revealed that increased transformation hysteresis is highly cutting speed related. Two hundred fifty m/min and 70 m/min cutting speed values resulted in 31.5 and 37.8 °C post-machining transformation hysteresis respectively. Compared to the unmachined sample, a minimal change in functional properties was achieved at the cutting speed of 250 m/min. Likewise, the lowest cutting speed (70 m/min) led to maximum subsurface hardening and deeper machining-induced layer according to metallurgical investigations. Residual austenite formation was evident on the subsurface of the machined specimens.

1 Introduction

The attention in the NiTi shape memory alloys (SMAs) in scientific studies and industrial applications is gaining momentum. These materials are capable of undergoing a reversible solid-state phase transformation process between high-temperature austenite phase and low-temperature martensite phase. Accordingly, functional behaviors (shape memory and pseudo-elasticity), which are the main reasons for the recognition of these materials as "unique," are obtained. In addition to the functional behaviors, NiTi SMAs possess corrosion resistance. These alloys have good mechanical properties such as high yield strength, high elastic deformation, superior recoverable elasticity, ductility, and good surface hardness. These make them very suitable for a great number of aerospace and biomedical applications. These high-value industrial applications demand components with a high level of dimensional precision as well as reliable functional properties. At this point, the manufacturing process renders a great significance.

Machining has been widely employed in the manufacturing of NiTi components owing to its capabilities in producing 3D complex shapes within very narrow dimensional and geometric tolerances. As documented by Kaya and Kaya, efforts for the improvement of machinability characteristics of NiTi SMAs have received considerable attention in the last two decades due to problems like severe tool wear, high cutting loads, affected surface integrity, poor chip handling, and burr formation [1]. It is known that these problems arise from the inherent properties of the alloy and the interactions between the cutting tool and the workpiece. Accordingly, the investigations in this issue have found that machining parameters and conditions have direct effects on these problems. By controlling these parameters, the mechanical and the thermal loads are also controlled. Among these, cutting speed is the most dominant one. According to Weinert and Petzoldt, increased cutting forces and tool wear were seen when the turning cutting speed was decreased below $Vc = 60$ m/min [2]. Biermann et al. reported that cutting

✉ Eren Kaya
erenkaya@eskisehir.edu.tr

1 Department of Mechanical Engineering, Eskisehir Technical University, Eskisehir 26555, Turkey

speed of $Vc = 50$ m/min resulted in the longest tool life with the least cutting force compared to $Vc = 30$ and 40 m/min in micro-drilling of NiTi alloy [3]. Similarly, Huang found that increase of the cutting speed over $Vc = 50$ m/min led to lower surface roughness, tool wear, and cutting forces in the end milling of NiTi [4]. Kaya and Kaya showed that it is possible to machine NiTi using a high cutting speed range with regard to tool life criteria [5]. Kuppuswamy and Yui investigated micro-milling characteristics of NiTi alloy with an aim to reduce cutting forces and burr formation [6]. It was shown that cutting forces and burr formation decrease dramatically when the cutting speed was increased above 15 m/min. This occurrence was attributed to phase transition from B2 to B19. Likewise, application of much-higher cutting speed (i.e., ultra-high-speed machining) was also reported to change machining characteristics due to ductile-to-brittle transformation of ductile work material [7]. In a more recent study, the effects of cutting parameters on surface characteristics were investigated [8]. Accordingly, cutting speed was found to be the most determinative factor on surface characteristics and midrange cutting speed ($Vc = 200$ m/min) along with minimum federate ($f = 0.08$ mm/rev) should be employed for optimal surface quality and subsurface hardening. Investigation of chip formation characteristics of NiTi revealed that there is a significant reduction in chip microhardness with an increase of cutting speed [9]. According to Altas et al., the most determinative factors on surface roughness and flank wear, when milling NiTi alloy, are nose radius and federate accordingly [10].

Kaynak et al. reported that cryogenic machining has also been demonstrated to be effective in achieving suppressed tool wear and cutting force [11]. Similarly, Zhao et al. investigated machinability characteristics of NiTi alloy under different cutting conditions (dry, flood cooling, and cryogenic cooling) using a wide range of cutting speed span ($Vc = 7.5–125$ m/min) [12]. The scholars reported that when the cutting speed is lower than $Vc = 33$ m/min, flood cooling is advantageous in cutting forces, tool wear, and surface roughness. At the highest cutting speed of the study ($Vc = 125$ m/min), the best machinability responses were obtained with cryogenic cooling.

According to Shokrani et al., optimization of process parameters in order to achieve a high level of productivity is not enough for the machining process [13]. Likewise, the multifunctional requirements of the NiTi components direct the manufacturing process to yield a minimum impact on the functional properties. As reported by Thakur and Gangopadhyay, machining has direct influences on surface integrity and functional properties [14]. This influence has been investigated in NiTi alloys by some researchers. Several authors have found that a decrease of cutting speed results in increased subsurface microhardness and hardened layer depth [4, 15, 16]. Huang documented that decrease

of cutting speed below $Vc = 100$ m/min led to a dramatic increase in the subsurface hardness in milling of NiTi [4]. According to Weinert et al., increase of cutting speed leads to minimal subsurface hardness of NiTi between drilling speed range of $Vc = 5$ to 60 m/min [16]. This phenomenon may be explained by subsurface work hardening (similar to other Ni and Ti alloys) and thermo-mechanical coupled phase transformation behaviors. The second one is highly material specific owing to phase transformation window (mostly being around room temperature and has not been very well explained yet). As pointed out by Kong et al., this renders a great significance in the machining of NiTi shape memory alloys [17]. According to Kaynak et al., cryogenic cooling–aided machining or using low cutting speed values results in residual austenite in the subsurface layer of the machined specimens [18]. Further investigations of these samples were reported to show that phase transformation properties (transformation enthalpy and temperatures) were severely affected. Similarly, Liu and Favier presented that the application of cold work significantly affects phase transformation temperatures [19]. These findings show that proper machining parameters and conditions should be employed in order to achieve desired functional properties.

The present literature offers an insight into machinability characteristics and machining-induced phase transformation responses of NiTi. Accordingly, the problems arise from both the in-process machinability characteristics (cutting force, tool wear, chip handling, etc.) and the post-machining behaviors (functional and surface integrity). To date, these problems have only been investigated under low to moderate cutting speed values using cemented carbide cutting tools. In light of the recent findings, especially concerning functional properties, the question of the suitability of high-speed machining of NiTi SMA arises. The aim of this study is to evaluate machinability and functional integrity and develop a better explanation of phase transformation behaviors of NiTi SMAs in high-speed machining. Cemented carbide and polycrystalline diamond (PCD) cutting tools were employed in a moderate to high cutting speed window. Tool wear, surface quality, microhardness, transformation temperatures, and transformation enthalpy were evaluated.

2 Materials and methods

The machining experiments were conducted as longitudinal turning. The machined specimen was room temperature martensitic NiTi alloy (Ni50Ti50, at.%). The workpiece was 25-mm diameter round bar. With the purpose of determining phase transformation temperatures and transformation enthalpy of the specimens, heating and cooling rate of 10 °C/min was used with the commercial differential scanning calorimetry (DSC, TA Instruments-DSC 25). Figure 1
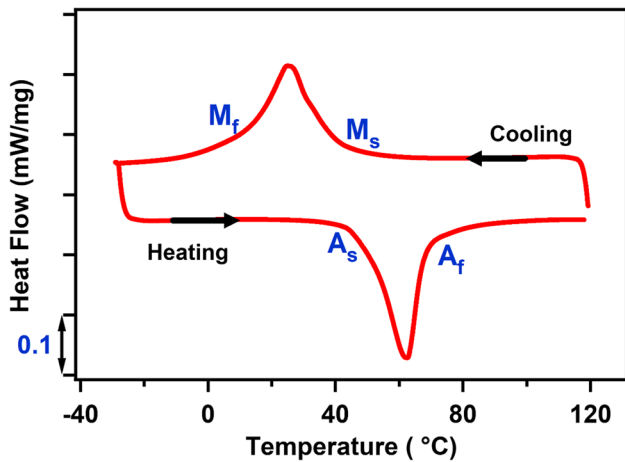
Fig. 1 DSC examination of the workpiece

shows the DSC graph with a full span of heating and cooling cycle. Accordingly, the martensite start (M_s), martensite finish (M_f), austenite start (A_s), and austenite finish (A_f) temperatures were detected as 38, 9, 50, and 68 °C, respectively. It is evident that the room temperature phase of the material is martensite. The experimental details are summarized in Table 1.

The cutting tools were C shape (80° Rhombic) with nose radii of 0.8 mm. The investigated cutting tool materials were multilayer PVD-coated carbide (Kennametal, KCU 10) and ultrafine grain size (0.5–1 µm) PCD (Kennametal, KD 1400). The grade of the carbide tool was selected regarding the manufacturer's statements through suitability for high-speed machining. Similarly, the purpose of PCD use is this material's proven high-speed machining capability in titanium alloys. Oosthuizen et al. showed that PCD tools surpassed carbide cutting tools in terms of cutting forces, surface finish, and tool life at elevated cutting speeds [20]. The ISO designation of the tool holder was TCLNL 2525. Additional geometric properties of the tools were tool cutting

edge angle of 95 deg., the side rake angle of -5 deg., the back rake angle of -5 deg., and clearance angle of 5 deg. The cutting edges of the cutting tools were round honed to 25-µm radii for carbide and chamfer honed to 5 µm for PCD (nearly perfectly sharp).

The turning experiments were operated on a CNC lathe with 22-KW spindle power. Figure 2 shows the machine tool setup. Constant depth of cut of $a_p = 0.2$ mm and feedrate of $f = 0.05$ mm/rev were used during all the machining experiments. The studies of Mehrpouya et al. [21] and Weinert and Petzoldt [2] in turning of NiTi indicate that moderate-to high-speed transition range can be designated between $Vc = 90$ and 120 m/min. According to Thakur et al. [22], this range was accepted at lower bounds (around $Vc = 40$ m/min) for Ni-based alloys. Four different cutting speed values were investigated in this study: $Vc = 70$, 130, 190, and 250 m/min. The dry cutting condition was used in all the experiments. As PCD tooling is rather sensitive to vibrations during machining, the holders were mounted on the tool post as short as possible to inhibit tool chatter.

Tool wear measurements were conducted after a longitudinal turning distance of 25 m employing a digital
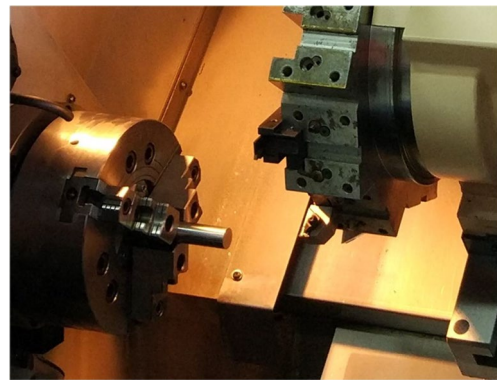

Fig. 2 Machine tool setup

Table 1 Experimental details

Items	Descriptions
Workpiece	Nickel-titanium shape memory alloy (Ni50Ti50, at.%) Round bar ø 25 mm
Machine tool	Horizontal CNC lathe (22 KW spindle power)
Cutting tool	ISO C shape insert (80° rhombic) with nose radii of 0.8 mm PVD coated carbide, PCD
Cutting speed (Vc)	70, 130, 190, 250 m/min
Feedrate (f)	0.05 mm/rev
Dept of cut (a_p)	0.2 mm
Cutting condition	Dry
Cutting strategy	Longitudinal turning
Measurements	Tool wear, surface roughness, transformation enthalpy, transformation temperature hysteresis, surface hardness

optical microscope. The cutting experiments with intervals of the above specified distance were advanced until any of the following measures is caught up: (1) maximum flank wear of $VB_{max} \geq 0.5$ mm, (2) average flank wear of $VB_a \geq 0.3$ mm, (3) notch wear of $VB_N \geq 0.6$ mm, or (4) catastrophic failure at the cutting edge of the insert. It should be noted that the size of the crater wear was lower than that of flank wear in all experiments. Measurements of the surface roughness were conducted with a surface profilometer (TESA, Rugosurf 20) after cutting with unworn tools.

Shear plane angle (ϕ) and shear strain (γ) were calculated for each cutting speed using well-known merchant equation [23]. For these calculations, actual chip thickness, uncut chip thickness, and cutting tool back rake angle values are used. Although not used as direct comparison criteria, these calculations are assumed to give a reasonable theoretical basis [24].

In the post-machining sample preparation procedure, the sample cross-section was cut from the stock machined with fresh cutting tools. The subsurface microhardness profile was measured with a microhardness tester device (Struers, Duramin 4). Ten measurements were performed for each depth level and the average was accepted. Functional integrity is evaluated in terms of transformation enthalpy and transformation temperatures. Prepared samples were analyzed with DSC employing a 10 °C/min heating and cooling rate.

3 Results and Discussion

3.1 Tool wear

Tool wear should be kept under control not only for increased productivity but also for achieving unaffected surface and functional characteristics. Machining of NiTi is characterized by severe flank wear, notch wear, and less dominantly rake wear modes. These are mainly originated from abrasive, adhesive, and diffusion wear mechanisms. Similar to other titanium alloys, material inheritances like high specific heat, poor thermal conductivity, and tendency to strain hardening [25] are major causes of rapid tool wear.

Tool life variations in terms of circumferential cutting distance are presented in Fig. 3. It is manifested that the PCD tool surpassed the carbide tool in the high cutting speed range. Carbide tool met the longest tool life of 750 m at the lowest cutting speed value ($Vc = 70$ m/min). As expected, this occurrence originated from well-known binder phase thermal softening in the cemented carbide. The upmost cutting life of the investigation with the tool life of 1725 m was yielded at $Vc = 130$ m/min with the PCD cutting tool. Further increase of the cutting speed led to a dramatic decrease in both of the cutting tool materials.

Tool wear images after 25-m circumferential cutting distance for $Vc = 130$ m/min cutting speed are given in Fig. 4. Here, most of the typical wear types observed in this study are present. It can be seen that abrasive groove marks are

Fig. 3 Tool life variations of the investigated tool materials for investigated cutting speed values
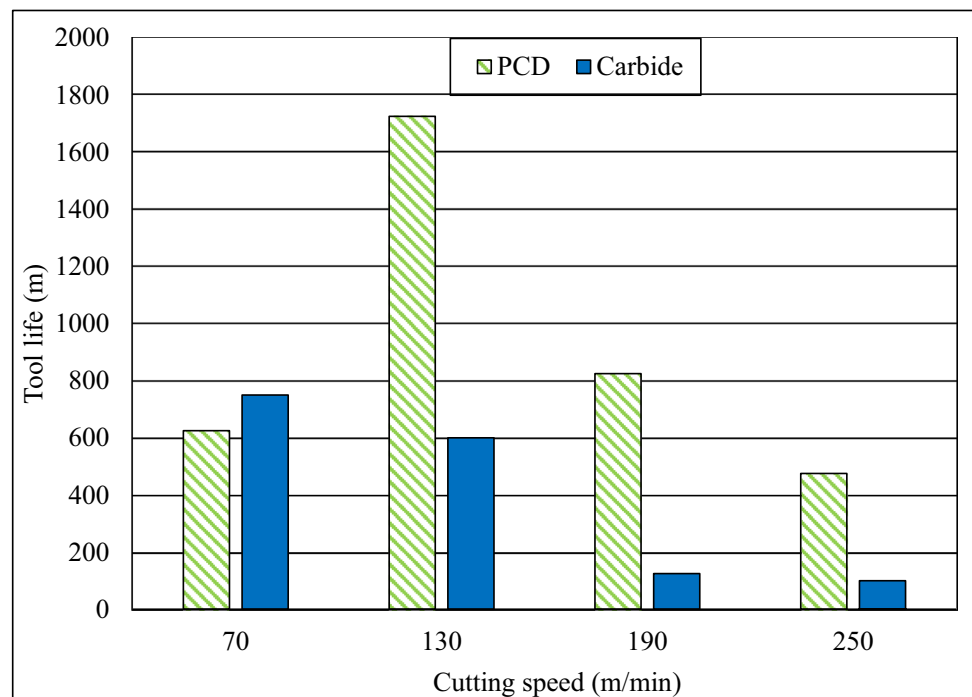
Fig. 4 Rake and flank images at $Vc = 130$ m/min following initial cutting distance, **a** flank face of the carbide, **b** rake face of the carbide, **c** flank face of the PCD, **d** rake face of the PCD
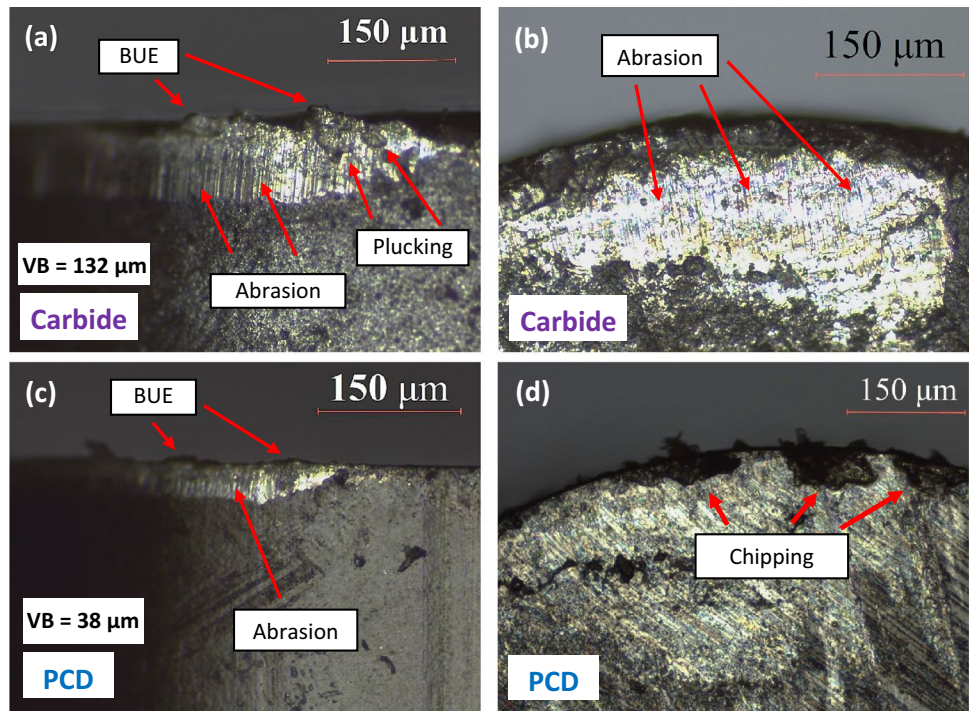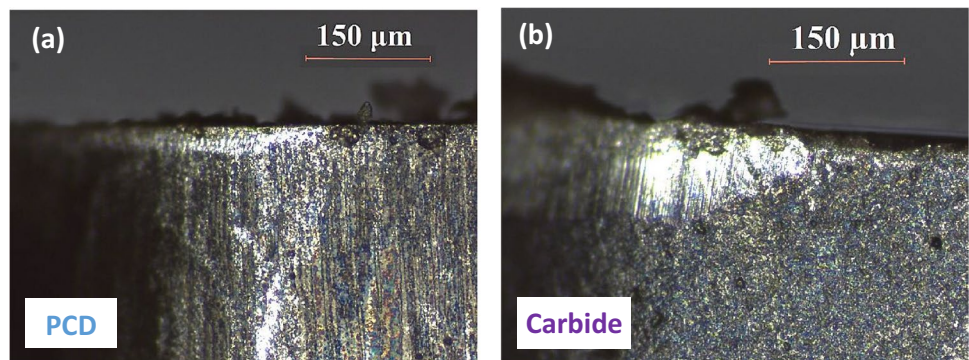

Fig. 5 Flank images at $Vc = 190$ m/min, **a** PCD tool, **b** carbide tool

evident on the flank and rake face of the carbide cutting tool as seen in Fig. 4a and b. This was observed in all investigated cutting speed values. Adhesion-driven plucking is evident on the flank face and lesser extend on the rake face. Adhesion also led to BUE formation, which was gradually decreased as the cutting speed was increased to the maximum. As shown in Fig. 5a and b, when the cutting speed was increased to $Vc = 190$ m/min, BUE was totally diminished for PCD and decreased remarkably for the carbide tool. The sharp decrease in tool life of the carbide at the cutting speed of $Vc = 190$ m/min was mainly caused by plastic deformation at the cutting edge. Figure 6 shows this occurrence on flank image. This originated from the thermal softening of the cutting tool at increased cutting speed values. Accordingly, further increase of cutting speed resulted in quicker tool wear with similar wear mechanisms. It should be noted that flank wear was always accompanied by coat flaking. In contrast
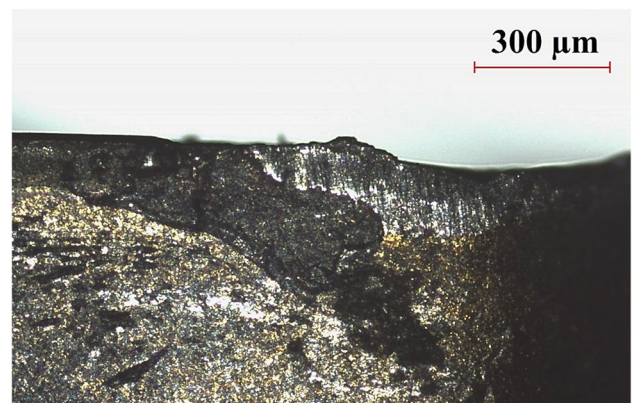

Fig. 6 Flank image of carbide tool at $Vc = 190$ m/min after 125-m cutting distance

to earlier findings by Kaynak et al. [11], little or no dominant notch wear was observed throughout the investigated cutting speed range. This occurrence was, most probably, a result of the investigated cutting speed range. According to Weinert et al., notch wear formation was eliminated when cutting speed value over $Vc = 70$ m/min was used in turning of NiTi [16].

PCD is the hardest cutting tool material known. Its high thermal conductivity and toughness compared to other super-hard cutting tools make it very suitable for cutting of some challenging to cut materials like titanium alloys. Although known as an abrasion resistant material due to its high hardness, abrasion marks were observed on the flank face of the PCD cutting tools throughout all investigated cutting speed values. This can be seen in Fig. 4c. The evidence suggests that these grooves resulted from fragments of the chipping at the cutting edge as seen in Fig. 4d. Li et al. reported that this type of wear was reported to be dominant in the high-speed machining of Ti6Al4V alloy [26]. Although the cutting tests were employed in a continuous cut manner, the adiabatic shearing effect of the material results in cyclic high thermal and mechanical loads during cutting. As a result, chipping takes place. The reason of the increase of the tool life at $Vc = 130$ m/min was most probably originated from the thermal softening of the workpiece because of the increased strain rate and hence cutting temperature. However, further increase of the cutting speed resulted in shorter tool life. This most probably resulted from the preeminence of tribo-chemical wear over mechanically activated wear, because cratering initiation on the rake face, after cutting speed of $Vc = 190$ m/min, along with flank wear led to edge weakening. These craters were clearly observed on the rake face. High cutting temperatures along with chip thinning, due to high cutting speed, most probably led to diffusion of carbon and titanium to form TiC. Figure 7 shows the effects of cutting speed on a shear plane angle and shear strain. Here, decrease of shear strain with increased cutting speeds indicates the chip thinning effect at the elevated cutting speeds. Li et al. reported similar findings of tribo-chemical wear in the machining of titanium alloys with PCD tools [26]. Parallel with those findings, although no EDS test was conducted, rake wear images (see Fig. 8) support this suggestion.

At the cutting speed of $Vc = 250$ m/min, more evident abrasion grooves were observed on the flank and rake face of the PCD tool. It is interpreted to happen that after a critical temperature atmospheric oxygen picked the titanium to form TiO_2 particles, which are quite hard and abrasive. Evidence suggests that this phenomenon also resulted in notching at the depth of the cut level. This oxidation driven notch wear initiated with a small notch and discoloration on the rake fake as seen in Fig. 9a. At the further cutting distances (see Fig. 9b, c), this notch grew and eventually led to catastrophic edge breakage as shown in Fig. 9d. According to Zoya and Krishnamurthy, this happens at a temperature of 800 °C. It appears that the sliding of these hard particles led to even more abrading effect [27].

The tool wear findings revealed that high-speed machining using PCD tools yielded favorable results. According to the previous work on the machining of NiTi alloy in the low cutting speed range using carbide cutting tools [11, 28], cutting speed values above 50 m/min result in quite high tool wear. In the present study, the wear behavior of the carbide tools is similar to these findings. Remarkably, the wear behavior of PCD tools differs from those. The superior wear results of the PCD tool of the present study do not support

Fig. 7 Effects of cutting speed on theoretical shear plane angle and shear strain for PCD cutting tool
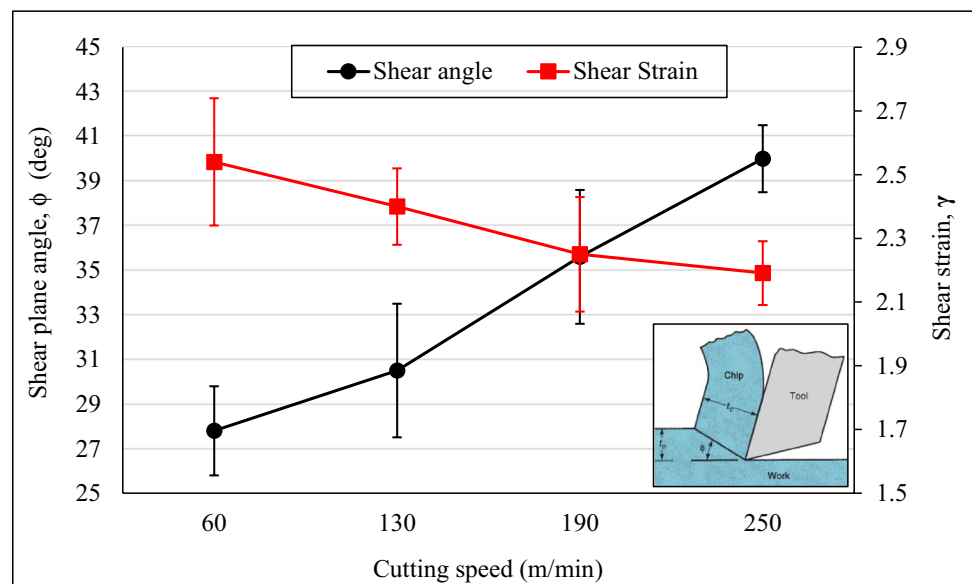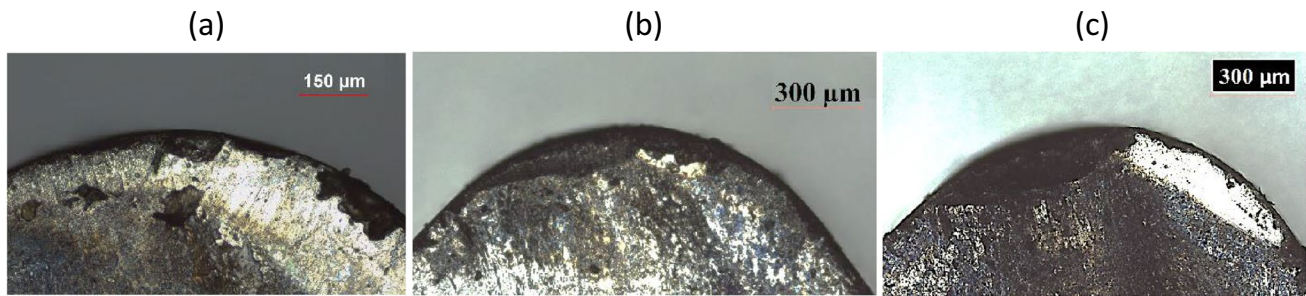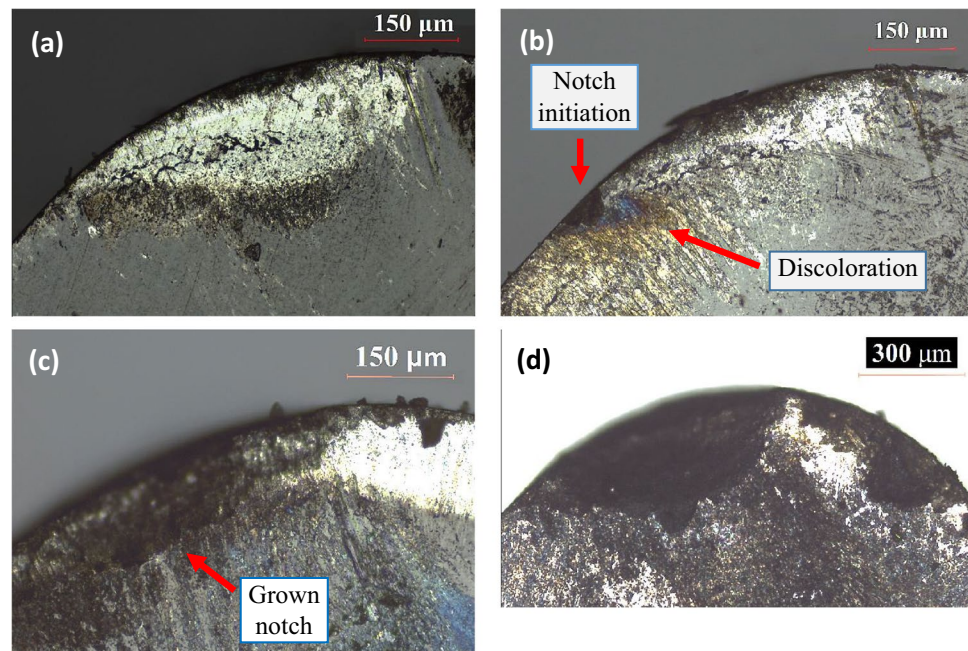
Fig. 8 Rake images of PCD cutting tool at $Vc = 190$ m/min after certain cutting distances, **a** 225 m, **b** 450 m, **c** 825 m

Fig. 9 Rake face of the PCD cutting tool at $Vc = 250$ m/min after certain cutting distances, **a** 25 m, **b** 100 m, **c** 375 m, **d** 475 m


previous research [16]. This contradiction was, most probably, resulted from cutting parameters or tool material grade, since there was, for PCD tool, quite short information on these factors in that study.

3.2 Surface roughness

Surface finish is a major element of surface integrity as it reflects fatigue life and functional integrity characteristics. The effect of the cutting speed variation on the surface roughness (Ra, μm) is presented in Fig. 10. Evidently, the trend of the surface roughness and cutting speed curve is very similar to that of tool wear for both of the tool materials. This similarity matches well with the findings of Huang [4], in the investigation of high-speed milling characteristics of NiTi. It would appear that surface finish was greatly influenced from tool wear or the reasons of tool wear and surface roughness are the same. These might

be cutting forces, machine tool vibrations, chip adherence, burr formation, strain hardening, or active phase effects. Although a smoother surface finish may be anticipated at the elevated cutting speed values owing to thermal softening, and hence less mechanical loads and strain hardening, generally the opposite effect is observed. Most probably, fragments due to chipping or tribo-chemical wear rubbed the tool-workpiece interface around the tool flank. This simultaneously led to an increasing trend in surface roughness and tool wear. As for the decrease in the surface roughness between $Vc = 70$ and 190 m/min for the PCD tool, it would appear that the minimum chipping combined with uninitiated chemical wear yielded the best surface quality. It should also be noted that the surface deterioration with the cutting speed increase is more obvious in the carbide tool. This finding is consistent with previous work on machining of NiTi Alloy using carbide tools and low speeds [29].

Fig. 10 Surface roughness variation with cutting speed
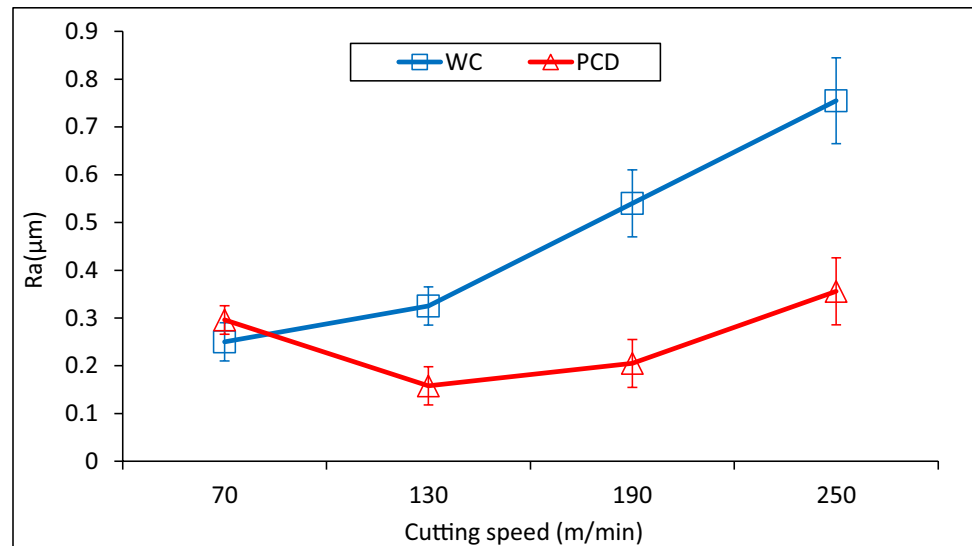
3.3 Phase transformation behaviors

Reversible solid-state phase transformation capability is the major superiority of the SMAs over the conventional structural alloys. The phase transformation behaviors are mainly influenced by alloy composition, microstructure, and mechanical and thermal load history of the material. Since the properties and the microstructure of the machining induced subsurface layer mainly depend on the thermo-mechanical influences of the machining operation, the ascertainment of optimum machining parameters is crucial.

Miller and Lagoudas documented that plastic deformation–induced dislocations increase the residual stress and this restraints the phase transformation [30]. As this stress-induced martensitic structure becomes residual, unless a heat treatment is applied, the transformation enthalpy (latent heat, ΔH), which is an apparent indicator of the amount of material undergoes phase transformation, decreases. Application of higher force and hence mechanical stress leads to more plastic deformation. This would enhance the stabilized martensite. According to Karaman et al., this occurrence originates especially from high dislocation densities stored in martensite plates and at the prior internal twin boundaries [31]. The scholars found that the reverse transformation temperatures (A_s and A_f) increased significantly in the samples deformed at room temperatures. The evidence from the study by Liu and Favier [19] suggests that deformation induced microstructure defects and stabilized martensite can be minimized with increased deformation temperature. Furthermore, it was found that thermal cycles had a diminishing effect on the stabilized martensite. These were attributed to the annihilation effect of overheating on the vacancies and the formation of different martensite variants (due to subsequent transformation cycles). These are free from impediment of the deformation-induced dislocations.

Figures 11 and 12 present the martensitic (M) and austenitic (A) transformation enthalpies of the machined specimens with PCD and WC cutting tools respectively. It should be noted that the DSC specimens were cut from the machined part after turning with unworn cutting tools. It is evident that a decrease of cutting speed leads to decreased transformation enthalpy. Machining with carbide and PCD cutting tools at $Vc = 70$ m/min ended up with measured austenitic transformation enthalpy of 11.6 and 13.8 j/gr, respectively, whereas ΔH of the as-received sample was 22.9 j/gr. At the highest cutting speed ($Vc = 250$ m/min), ΔH of the samples cut with PCD and carbide was 20.72 and 19.95 j/gr respectively. This resulted from higher cutting forces and hence shear stress at the lower cutting speed values (thermal softening phenomena). Consequently, stress-induced martensite formation and increased dislocation densities are formed. Owing to the essence of metal cutting, an increase of the cutting speed results in decreased cutting forces and stresses and increased cutting temperatures. Referring back to Fig. 7, this phenomenon can be observed from the shear plane angle and cutting speed curve. Here, the increased shear plane angle at the elevated cutting speed values indicates a smaller shear plane and accordingly lower cutting force and energy [32]. This led to less restricted phase transformation behaviors. As in a good correlation with previous studies discussed above, these results originated from (1) less stress-induced stabilized martensite and dislocation densities and (2) stress annihilation and crystal structure vacancy recovery effects. Analogously, in the machining of NiTi at the low cutting speed band, similar cutting speed and transformation enthalpy behaviors were documented [15, 18]. Accordingly, when the cutting speed was decreased to $Vc = 6.25$ m/min, the ΔH was reported to nearly totally diminish (3.4 j/gr). It should also be noted that measured transformation enthalpy after machining with each cutting speed for both

Fig. 11 Transformation enthalpy results after machining with PCD cutting tools
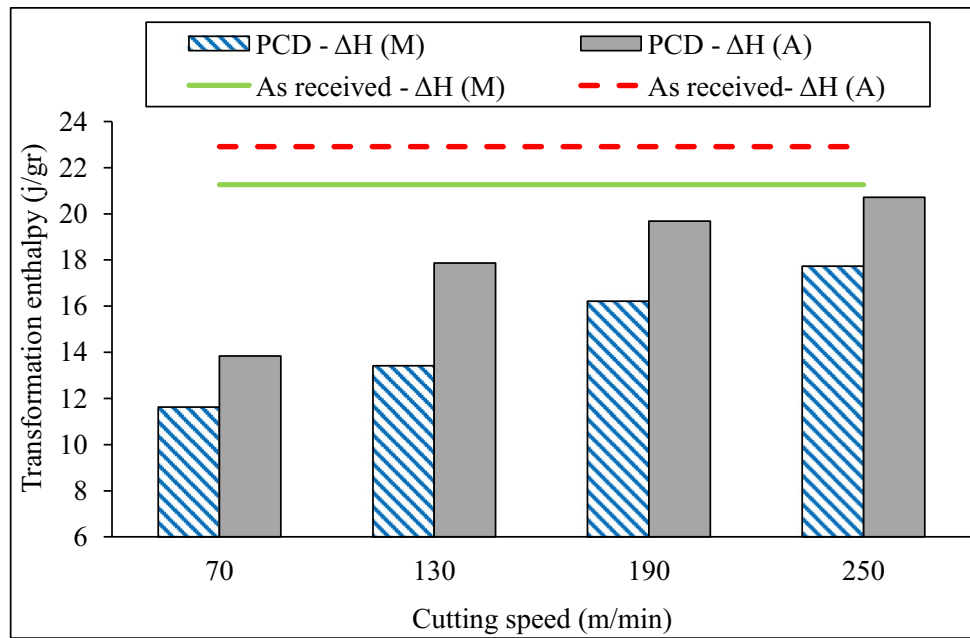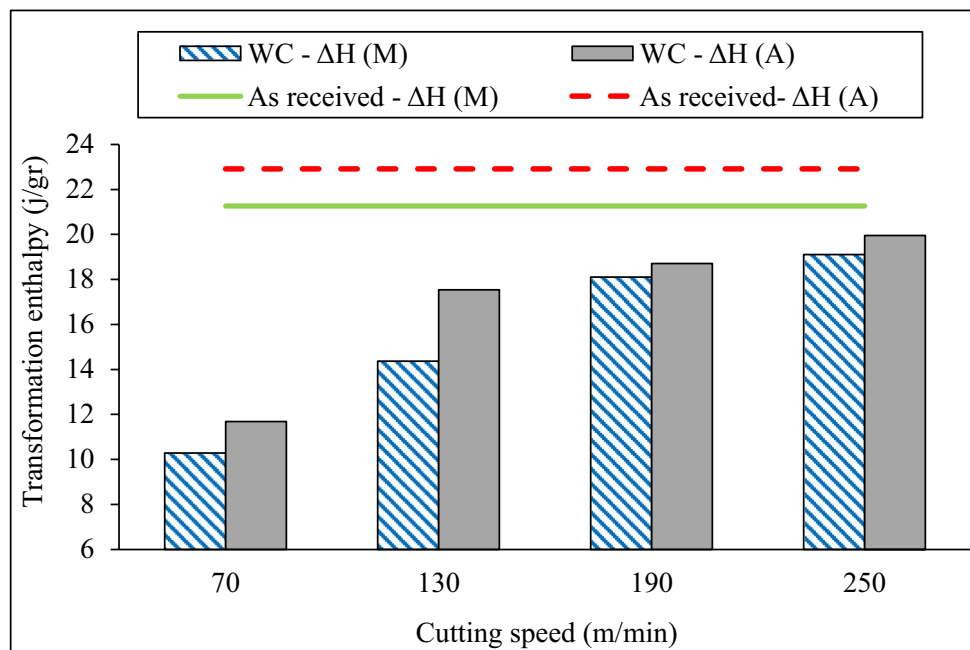

Fig. 12 Transformation enthalpy results after machining with WC cutting tools


cutting tools are quite close. The slight difference in ΔH is the greatness of the PCD compared to WC, and around 1 j/gr. This was attributed to the PCD tool's cutting edge being sharper. Since sharper edge yields less cutting force, and less mechanical load, hence fewer stabilized martensite is expected.

In this study, the term thermal hysteresis stands for the interval between A_f and M_s temperatures. Large transformation hysteresis was associated with austenite/martensite interface incompatibility and poor functional integrity properties. Phase transformation thermal hysteresis is caused by

the dissipation of energy frictionally and thermally. According to Ramaiah et al., low thermal hysteresis indicates low irreversible energy levels of phase transformation [33]. McCormick and Liu conducted a thermodynamic analysis of phase transformation on NiTi with and without applied mechanical loads [34]. They explained the origination of irreversible energy from energy loss due to friction and plastic deformation during the phase transformation regarding Gibb's energy equation. The motion of twin interfaces and phase/twin boundaries are mainly responsible for energy loss. According to Dirand et al., M_s point is where the

Fig. 13 Transformation hysteresis results after machining with WC and PCD cutting tools
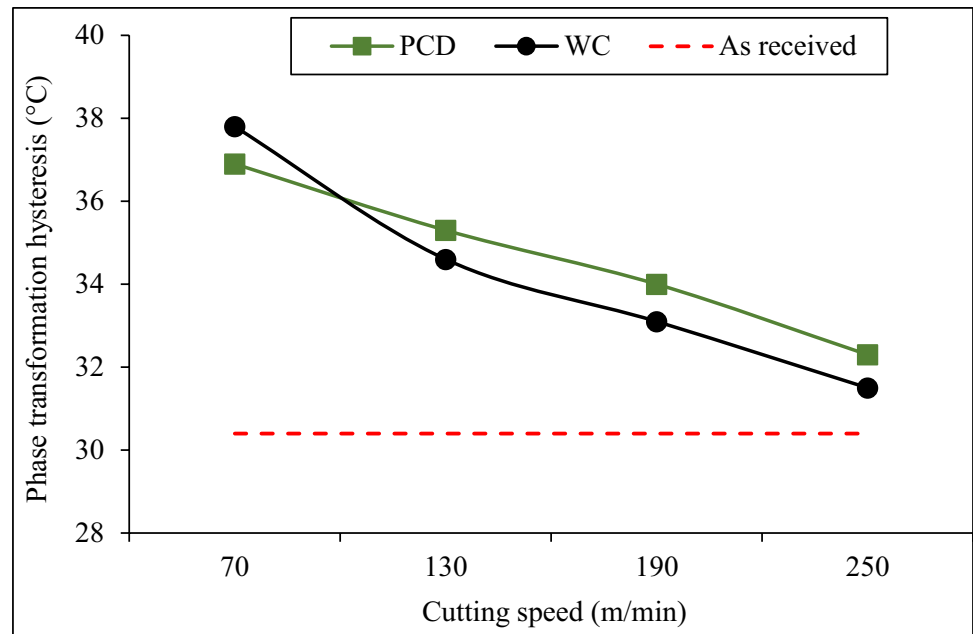
maximum lattice internal friction exists and this is attributed to the nature of the microstructure of the martensite [35]. Lin et al. were among the first to demonstrate that cold work shifts reverse martensitic temperatures to higher values [36]. This phenomenon was confirmed by Karaman et al. [31]. The scholars concluded that the cold work does not alter the martensitic transformation temperatures; however, it shifts forward the austenitic transformation temperatures in NiTi. This situation, as explained above, arises from internal stress, friction, and dislocations and this leads to increased

transformation hysteresis ($A_f − M_s$). The amount of forward shift in austenitic transformation temperatures, and hence the increase in the hysteresis, mainly depends on deformation mode, intensity, and temperature.

Figure 13 presents the influences of cutting speed variation on the transformation temperature hysteresis of the NiTi. The results revealed that the machining process altered the transformation hysteresis, throughout the investigated cutting speed range. It is evident that this increase is highly cutting speed related. The increase of cutting speed resulted in

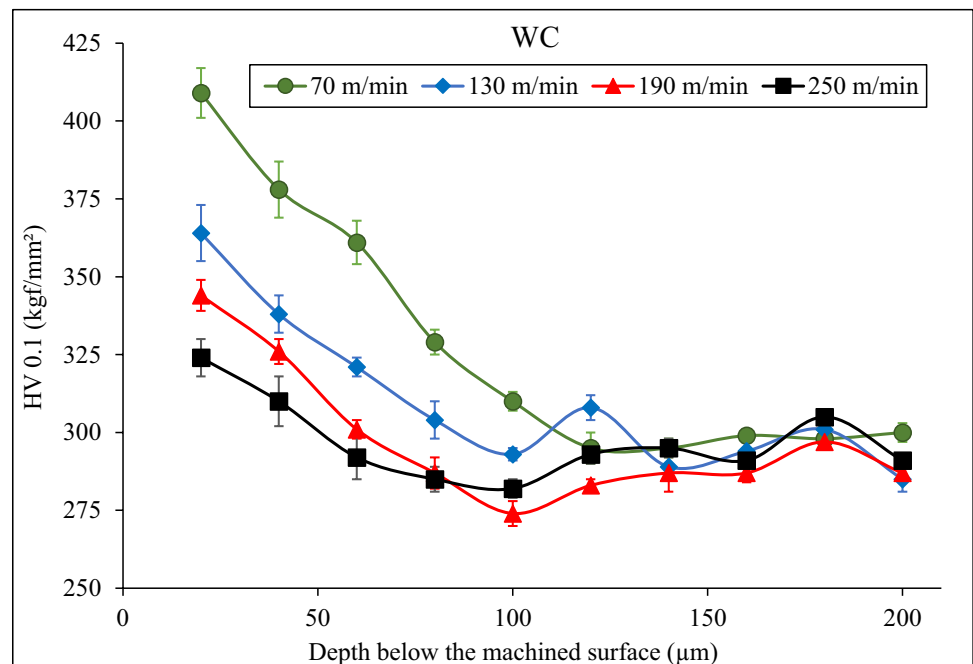**Fig. 14** Subsurface microhardness variation after machining with WC tool
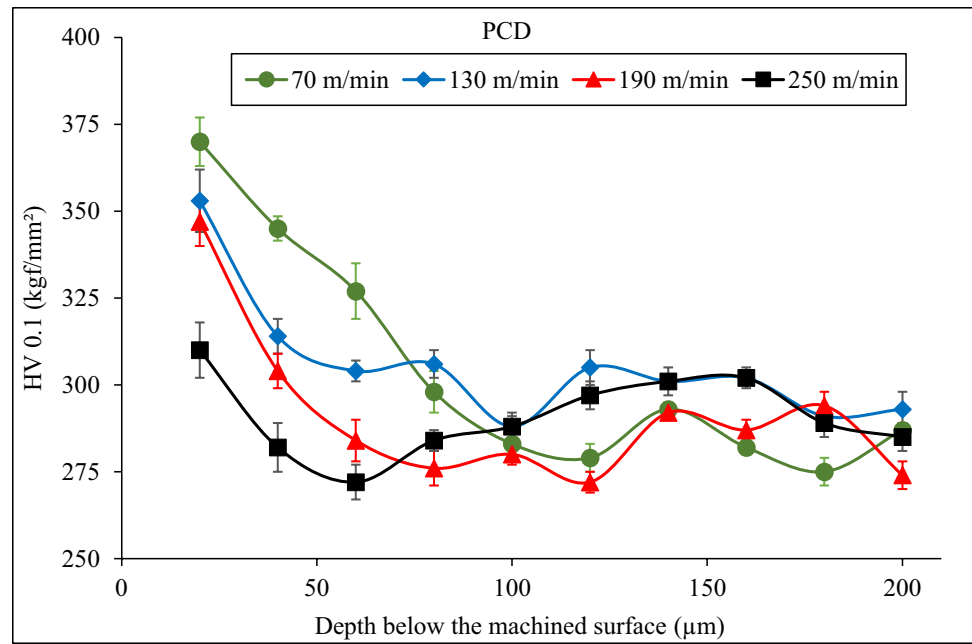
**Fig. 15** Subsurface microhardness variation after machining with PCD tool

less pronounced increase in the phase transformation hysteresis. There is not a very significant difference between PCD and WC. Compared to the as-received sample, the increase in the hysteresis is about 7 °C at $Vc = 70$ m/min, whereas it is only around 1.5 °C at $Vc = 250$ m/min. In a similar manner to transformation enthalpy results, relatively high cutting stress and, in turn, deformation and dislocation densities at the lower cutting speed values were responsible for this. In the previous work on machining of NiTi in lower cutting speeds, alterations in austenite start and finish temperatures were reported [18], because increased elastics strains and internal friction energy delay the phase transformation onset. Increase of cutting speed results in decreased cutting stress and elevated cutting temperatures. These findings match quite well with the previous investigations focusing on the

influences of cold work and annealing temperature on NiTi. Hamilton et al. reported that increase of external stress leads to substantially increased thermal hysteresis (up to 60 °C) in low nickel NiTi alloy [37]. As documented by Mitwally and Farag [38], an increase of percentage of cold rolling not only increases the volume fraction of stabilized martensite but also decreases the superelasticity.

3.4 Subsurface hardness

Changes in subsurface hardness compared to base material indicate some machining-induced alterations in the microstructure and mainly caused by mechanically induced strain hardening. Figures 14 and 15 show subsurface microhardness variation as a function of depth from the machined

Fig. 16 Cross-section images after machining with PCD cutting tool with cutting speeds of **a** $Vc = 70$ m/min, **b** $Vc = 250$ m/min

(a) (b)
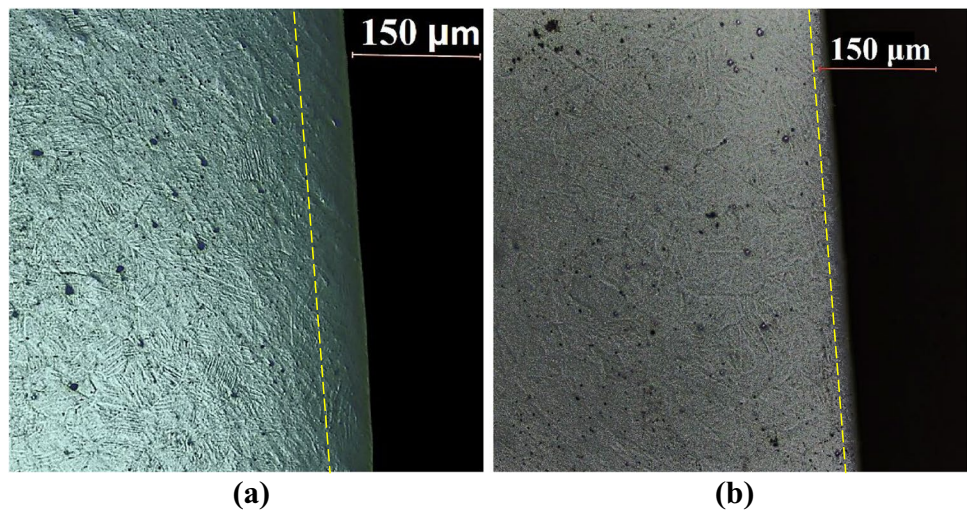
surface at the investigated cutting speed values after machining with fresh cutting tools. It should be noted that the hardening effects of the investigated cutting tool materials are similar. As expected, the hardness decreases with increased depth value and reaches the parent material at around a depth of 140 μm. It is obvious that the hardness value is significantly affected from cutting speed. The lowest cutting speed resulted in the greatest hardness in the subsurface zone, whereas the highest cutting speed resulted in the lowest with a value close to the base material. Accordingly, an increase of cutting speed led to less subsurface hardening as reported in the literature as mentioned before. This behavior, parallel to the phase transformation behavior findings, was attributed to decreased cutting stress and twin/dislocation annihilation effect of the elevated cutting temperatures at the higher cutting speed values.

These arguments can be supported by cross-sectional microstructure of the machined specimens presented in Fig. 16. Here, the subsurface machining-induced zone shows the disappearance of martensite twins which belong to the base material structure in both of the figures. This zone is deeper in the low-speed-cut specimen and diagnosed as residual austenite, as it is also known that austenitic NiTi has a higher hardness value. During the machining, the austenitic phase transformation took place. Although the samples cool down below the martensitic phase transformation temperatures after machining, the internal stress prevents this zone from returning to the martensitic state. Similar to stabilized martensite, this structure is accompanied by residual strain. In the mico-end milling of NiTi, similar behavior was reported by Picquart et al. [39]. Liu and Favier documented that a significant amount of residual austenite exists in the deformed martensitic NiTi according to X-ray measurements [19]. The scholars linked this finding to changes in transformation enthalpies and irreversible energies. As seen in Fig. 16, it is obvious that high cutting speed resulted in a narrower residual austenite layer.

4 Conclusions

In this experimental study, NiTi SMA was machined in the high cutting speed order using carbide and PCD cutting tools. Accordingly, the following conclusions can be drawn:

- Tool wear results indicate that tool wear mechanisms are cutting speed dependent. The higher range of the cutting speed values initiated tribo-chemical wear.

- Exceptional tool life is achieved with PCD tool at the cutting speed of $Vc = 130$ m/min. The surface quality behavior was very similar to tool life variation.
- The indicators of functional integrity showed that they are less impaired when higher cutting speed values are employed.
- Compared to unmachined material, minimal changes in transformation enthalpies, transformation hysteresis, and subsurface hardness were achieved with the highest cutting speed of the study.
- Machining with carbide and PCD cutting tools at $Vc = 70$ m/min ended up with measured austenitic transformation enthalpy of 11.6 and 13.8 j/gr, respectively, whereas ΔH of the as-received sample was 22.9 j/gr. Although similar findings were reported before in lower cutting speed range, severe tool wear was the limiting factor for use of high cutting values.

Data availability The datasets generated during and/or analysed during the current study are available from the corresponding author on reasonable request.

Code availability Not applicable.

Declarations

Ethics approval Not applicable.

Consent to participate Not applicable.

Consent for publication Not applicable.

Competing interests The authors declare no competing interests.

References

1. Kaya E, Kaya İ (2019) A review on machining of NiTi shape memory alloys: the process and post process perspective. Int J Adv Manuf Technol 100(5):2045–2087. https://doi.org/10.1007/s00170-018-2818-8
2. Weinert K, Petzoldt V (2004) Machining of NiTi based shape memory alloys. Mater Sci Eng A 378(1):180–184. https://doi.org/10.1016/j.msea.2003.10.344
3. Biermann D, Kahleyss F, Krebs E, Upmeier T (2011) A study on micro-machining technology for the machining of NiTi: five-axis micro-milling and micro deep-hole drilling. J Mater Eng Perform 20(4):745–751. https://doi.org/10.1007/s11665-010-9796-9

4. Huang H (2004) A study of high-speed milling characteristics of nitinol. Mater Manuf Processes 19(2):159–175. https://doi.org/10.1081/AMP-120029849

5. Kaya E, Kaya İ (2020) Tool wear progression of PCD and PCBN cutting tools in high speed machining of NiTi shape memory alloy under various cutting speeds. Diamond and Related Materials 105(107810). https://doi.org/10.1016/j.diamond.2020.107810

6. Kuppuswamy R, Yui A (2015) High-speed micromachining characteristics for the NiTi shape memory alloys. Int J Adv Manuf Technol 93:11–21. https://doi.org/10.1007/s00170-015-7598-9

7. Wang B, Liu Z, Su G, Song Q, Ai X (2015) Investigations of critical cutting speed and ductile-to-brittle transition mechanism for workpiece material in ultra-high speed machining. Int J Mech Sci 104:44–59. https://doi.org/10.1016/j.ijmecsci.2015.10.004

8. Wang G, Liu Z, Huang W, Wang B, Niu J (2019) Influence of cutting parameters on surface roughness and strain hardening during milling NiTi shape memory alloy. Int J Adv Manuf Technol 102(5):2211–2221. https://doi.org/10.1007/s00170-019-03342-9

9. Zhao Y, Li J, Guo K, Sivalingam V, Sun J (2020) Study on chip formation characteristics in turning NiTi shape memory alloys. J Manuf Process 58:787–795. https://doi.org/10.1016/j.jmapro.2020.08.072

10. Altas E, Gokkaya H, Karatas MA, Ozkan D (2020) Analysis of surface roughness and flank wear using the taguchi method in milling of NiTi shape memory alloy with uncoated tools. Coatings 10(12):1259

11. Kaynak Y, Karaca HE, Noebe RD, Jawahir IS (2013) Analysis of tool-wear and cutting force components in dry, preheated, and cryogenic machining of NiTi shape memory alloys. Procedia CIRP 8(Supplement C):498–503. https://doi.org/10.1016/j.procir.2013.06.140

12. Zhao Y, Guo K, Li J, Sun J (2021) Investigation on machinability of NiTi shape memory alloys under different cooling conditions. Int J Adv Manuf Technol 116(5):1913–1923. https://doi.org/10.1007/s00170-021-07563-9

13. Shokrani A, Dhokia V, Newman ST (2016) Investigation of the effects of cryogenic machining on surface integrity in CNC end milling of Ti–6Al–4V titanium alloy. J Manuf Process 21:172–179. https://doi.org/10.1016/j.jmapro.2015.12.002

14. Thakur A, Gangopadhyay S (2016) State-of-the-art in surface integrity in machining of nickel-based super alloys. Int J Mach Tools Manuf 100:25–54. https://doi.org/10.1016/j.ijmachtools.2015.10.001

15. Kaynak Y, Karaca H, Jawahir I (2015) Cutting speed dependent microstructure and transformation behavior of NiTi alloy in dry and cryogenic machining. J Mater Eng Perform 24(1):452–460. https://doi.org/10.1007/s11665-014-1247-6

16. Weinert K, Petzoldt V, Kötter D (2004) Turning and drilling of NiTi shape memory alloys. CIRP Ann Manuf Technol 53(1):65–68. https://doi.org/10.1016/S0007-8506(07)60646-5

17. Kong MC, Axinte D, Voice W (2011) Challenges in using waterjet machining of NiTi shape memory alloys: an analysis of controlled-depth milling. J Mater Process Technol 211(6):959–971. https://doi.org/10.1016/j.jmatprotec.2010.12.015

18. Kaynak Y, Huang B, Karaca H, Jawahir I (2017) Surface characteristics of machined NiTi shape memory alloy: the effects of cryogenic cooling and preheating conditions. J Mater Eng Perform 26(7):3597–3606. https://doi.org/10.1007/s11665-017-2791-7

19. Liu Y, Favier D (2000) Stabilisation of martensite due to shear deformation via variant reorientation in polycrystalline NiTi. Acta Mater 48(13):3489–3499

20. Oosthuizen GA, Akdogan G, Treurnicht N (2011) The performance of PCD tools in high-speed milling of Ti6Al4V. Int J Adv Manuf Technol 52(9):929–935. https://doi.org/10.1007/s00170-010-2804-2

21. Mehrpouya M, Shahedin AM, Dawood SDS, Ariffin AK (2017) An investigation on the optimum machinability of NiTi based shape memory alloy. Mater Manuf Processes 32(13):1497–1504. https://doi.org/10.1080/10426914.2017.1279290

22. Thakur DG, Ramamoorthy B, Vijayaraghavan L (2009) Study on the machinability characteristics of superalloy Inconel 718 during high speed turning. Mater Des 30(5):1718–1725. https://doi.org/10.1016/j.matdes.2008.07.011

23. Merchant ME (1945) Mechanics of the metal cutting process. II. Plasticity conditions in orthogonal cutting. J Appl Phys 16(6):318–324

24. Kuppuswamy R, Mkhize N (2017) Near ductile regime machining of tungsten carbide insert through control of cutting speed parameter while using a poly-crystalline diamond tool. Procedia Manuf 8:549–556. https://doi.org/10.1016/j.promfg.2017.02.070

25. Liu Y, Shan L, Shan J, Hui M (2019) Experimental study on temperature evolution and strain rate effect on phase transformation of TiNi shape memory alloy under shock loading. Int J Mech Sci 156:342–354. https://doi.org/10.1016/j.ijmecsci.2019.04.005

26. Li A, Zhao J, Wang D, Zhao J, Dong Y (2013) Failure mechanisms of a PCD tool in high-speed face milling of Ti–6Al–4V alloy. Int J Adv Manuf Technol 67(9):1959–1966. https://doi.org/10.1007/s00170-012-4622-1

27. Zoya Z, Krishnamurthy R (2000) The performance of CBN tools in the machining of titanium alloys. J Mater Process Technol 100(1–3):80–86. https://doi.org/10.1016/S0924-0136(99)00464-1

28. Kaynak Y, Karaca H, Noebe R, Jawahir I (2013) Tool-wear analysis in cryogenic machining of NiTi shape memory alloys: a comparison of tool-wear performance with dry and MQL machining. Wear 306(1):51–63. https://doi.org/10.1016/j.wear.2013.05.011

29. Kaynak Y (2014) Machining and phase transformation response of room-temperature austenitic NiTi shape memory alloy. J Mater Eng Perform 23(9):3354–3360. https://doi.org/10.1007/s11665-014-1058-9

30. Miller DA, Lagoudas DC (2001) Influence of cold work and heat treatment on the shape memory effect and plastic strain development of NiTi. Mater Sci Eng A 308(1–2):161–175. https://doi.org/10.1016/S0921-5093(00)01982-1

31. Karaman I, Karaca HE, Luo Z, Maier H (2003) The effect of severe marforming on shape memory characteristics of a Ti-rich NiTi alloy processed using equal channel angular extrusion. Metall Mater Trans A 34(11):2527–2539

32. Warsi SS, Jaffery SHI, Ahmad R, Khan M, Ali L, Agha MH, Akram S (2018) Development of energy consumption map for orthogonal machining of Al 6061-T6 alloy. Proceedings of the Institution of Mechanical Engineers, Part B: Journal of Engineering Manufacture 232 (14):2510-2522. https://doi.org/10.1177/0954405417703424

33. Ramaiah K, Saikrishna C, Bhaumik S (2014) Ni24.7 Ti50.3 Pd25.0 high temperature shape memory alloy with narrow thermal hysteresis and high thermal stability. Mater Des (1980-2015) 56:78–83. https://doi.org/10.1016/j.matdes.2013.10.079

34. McCormick PG, Liu Y (1994) Thermodynamic analysis of the martensitic transformation in NiTi—II. Effect of transformation cycling. Acta Metall Mater 42(7):2407–2413. https://doi.org/10.1016/0956-7151(94)90319-0

35. Dirand L, Nó ML, Chastaing K, Denquin A, Juan JS (2012) Internal friction and dynamic modulus in Ru-50Nb

ultra-high temperature shape memory alloys. Appl Phys Lett 101(16):161909. https://doi.org/10.1063/1.4761475

36. Lin H, Wu S-K, Chou T, Kao H (1991) The effects of cold rolling on the martensitic transformation of an equiatomic TiNi alloy. Acta Metall Mater 39(9):2069–2080. https://doi.org/10.1016/0956-7151(91)90177-3

37. Hamilton RF, Sehitoglu H, Chumlyakov Y, Maier HJ (2004) Stress dependence of the hysteresis in single crystal NiTi alloys. Acta Mater 52(11):3383–3402. https://doi.org/10.1016/j.actamat.2004.03.038

38. Mitwally ME, Farag M (2009) Effect of cold work and annealing on the structure and characteristics of NiTi alloy. Mater Sci Eng A 519(1):155–166. https://doi.org/10.1016/j.msea.2009.04.057

39. Piquard R, D'Acunto A, Laheurte P, Dudzinski D (2014) Micro-end milling of NiTi biomedical alloys, burr formation and phase transformation. Precis Eng 38(2):356–364. https://doi.org/10.1016/j.precisioneng.2013.11.006